Translational Stroke Research
https://doi.org/10.1007/s12975-022-01074-9

RESEARCH

The Role of Neutrophil Extracellular Traps in Early Microthrombosis and Brain Injury After Subarachnoid Hemorrhage in Mice

Xiaoke Hao[1,2] · Zongwei Zeng[1] · Liang Liang[1] · Zhou Feng[1] · Wu Li[3] · Binyuan Xiong[1] · Peiwen Guo[1] · Qiang Zhang[1] · Yujie Chen[1] · Hua Feng[1] · Zhi Chen[1]

Received: 12 April 2022 / Revised: 4 August 2022 / Accepted: 5 August 2022

Abstract

Microthrombosis plays an important role in secondary brain injury after experimental subarachnoid hemorrhage (SAH), but the specific mechanism of microthrombosis remains unclear. The purpose of this study was to investigate the role of neutrophil extracellular traps (NETs) in microthrombosis after SAH. SAH was induced in male C57BL/6 mice using an endovascular perforation technique. The marker protein of NETs, citrullinated histone H3 (CitH3), was significantly elevated in the cerebral cortex after SAH, and was co-labeled with microthrombi. Both depletion of neutrophils by anti-Ly6G antibody and DNase I treatment significantly reduced the formation of NETs and microthrombi, and ameliorated neurological deficits, brain edema, BBB disruption, and neuronal injury at 24 h after SAH induction. Cerebral hypoperfusion in the first hours after SAH is a major determinant of poor neurological outcome; in this study, we found that DNase I treatment significantly improved the restoration of early cortical perfusion after SAH. In addition, DNase I treatment also significantly attenuated cerebrospinal fluid (CSF) flow after SAH, which was associated with the diffusion barrier caused by microthrombi in the paravascular space after SAH. In conclusion, NETs are associated with early microthrombosis after SAH; they may be a novel therapeutic target for early brain injury (EBI) after SAH.

Keywords Microthrombosis · Subarachnoid hemorrhage · Neutrophil extracellular traps · Early brain injury

Introduction

Subarachnoid hemorrhage (SAH) is a devastating disease with high mortality and morbidity rates in patients [1, 2]. Evidences have indicated that early brain injury (EBI), which occurs within 72 h following cerebral aneurysm rupture, plays a crucial role in the outcome of SAH [3, 4]. Various mechanisms including microvascular thrombosis have been implicated in the pathogenesis of EBI after SAH [5]. Microthrombosis was found after SAH in patients and in experiment animal models; the number of microthrombi correlated with blood-brain barrier (BBB) disruption, early cerebral cortical hypoperfusion, and neuronal injury, but the mechanisms of microthrombus formation have not yet been fully elucidated [6–8].

Neutrophil extracellular traps (NETs) are a meshwork of chromatin fibers and antimicrobial peptides that are extruded by neutrophils and play important roles in many noninfectious diseases [9]. Recently, the formation of NETs has also been reported to be involved in the pathological processes of various central nervous system (CNS) diseases, such as SAH, ischemic stroke, and traumatic brain injury (TBI) [2, 10, 11]. In particular, the formation of citrullinated histone H3 (CitH3; the marker protein of NETs) in neutrophils is associated with adverse consequences. Moreover, NETs have been found to be implicated in thrombosis, which contribute to platelet aggregation and thrombus formation [12, 13]. Previous studies showed that the formation of NETs has been proposed as one of the mechanisms to

✉ Zhi Chen
zhichen@tmmu.edu.cn

1 Department of Neurosurgery, Southwest Hospital, Army Military Medical University (Third Military Medical University), No. 30 Gaotanyan Street, Chongqing 400038, China

2 Department of Neurosurgery, The Affiliated Huaihai Hospital of Xuzhou Medical University, Xuzhou 221000, China

3 Department of Geriatrics and Special Service Medicine, Southwest Hospital, Army Military Medical University (Third Military Medical University), Chongqing 400038, China

Published online: 13 August 2022

explain cancer-associated thrombosis; the infusion of DNase I, which degrades extracellular DNA and thereby NETs, can reduce the thrombus formation in tumor-bearing mice. NETs also play an important role in the formation of deep vein thrombosis (DVT); inhibiting NETs significantly suppressed DVT growth [14, 15]. Recently, researchers also found that NETs associate with microthrombus formation and platelet deposition in COVID-19 patients [16]. With this background, we proposed the hypothesis that the NETs were involved in the formation of SAH-induced microthrombi. First, we established an endovascular perforation model of SAH in mice and found the formation of NETs in the brain was significantly increased after SAH. Second, we identified the temporal patterns and localization of NETs after SAH and found NETs are consistent with microthrombi in location. At last, we demonstrated that DNase I treatment and neutrophil depletion can suppress NET formation and microthrombosis, and ameliorate neurological deficits, brain edema, BBB disruption, and neuronal injury. In addition, cerebral hypoperfusion in the first hours after SAH is a major determinant of poor neurological outcome, and previous studies have suggested that this may be associated with early microthrombosis after SAH [17, 18]. In this study, we found that DNase I treatment significantly improved the restoration of early cortical perfusion after SAH.

Blocking of cerebrospinal fluid (CSF) flow is one of the severe neurological complications after SAH [19, 20]. The paravascular space is a complex system that ensures the exchanges between the extracellular space and CSF contained in the subarachnoid space allowing the clearance of macromolecules and metabolic waste from the brain parenchyma [21]. It has been demonstrated that CSF is pumped into the brain along the periarterial space and disperses into the neuropil [21, 22]. Then, extracellular fluid will leave the brain along the perivenous spaces, followed by drainage along cranial nerves. At last, cervical glymphatic and meningeal vessels will collect the fluid and convey it [23]. When blood flows out of the vasculature and into the paravascular space during SAH, the coagulation cascade would be initiated, leading to thrombosis and blockade of CSF flow [24]. In the present study, we found that administration of DNase I restored CSF flow in early SAH. So we guessed that microthrombosis in the paravascular space might also be related to NETs.

Materials and Methods

Animals

All experimental procedures were approved by the Ethics Committee of the Army Medical University (Third Military Medical University), and was performed in accordance with the guidelines in the National Institutes of Health (NIH) Guide for the Care and Use of Laboratory Animals, and followed the ARRIVE guidelines. Two hundred and fifty-five adult male C57BL/6 mice weighing 22 to 28 g were provided by the Experimental Animal Center of the Army Medical University. Mice were acclimated in a reversed 12-h dark/12-h light cycle environment and provided with free access to water and food.

Experimental Design

The study contained four experiments, which were designed as follows and in Supplemental Fig. 1.

Experiment 1

To investigate the time course and cell location of NETs after SAH, 20 mice were randomly divided into the following five groups ($n = 4$/group): sham, 4 h after SAH, 12 h after SAH, 24 h after SAH, and 48 h after SAH. CitH3 protein expression was detected by western blot in the cortex isolated from the ipsilateral/left hemisphere. Additionally, 6 mice from sham and 24 h after SAH groups ($n = 3$/group), were used for double immunofluorescence staining to confirm the spatial distribution of NETs and microthrombi in the cortex. The time points were selected based on our pre-experimental results and previous study report, in which the level of NETs peaked at 24 h post-SAH in the brain [2].

Experiment 2

To elucidate the effect of neutrophil depletion treatment on EBI, 72 mice were randomly divided into three groups ($n = 24$/group): sham, SAH + vehicle (saline), and SAH + anti-Ly6G antibody. For neutrophil depletion, anti-Ly6G antibody (1A8 BioLegend 127,649) was intravenously injected into mice at a dose of 5 μg/g mouse at 24 h before SAH [25, 26]. SAH severity, neurological scores (beam balance and modified Garcia tests), brain water content, Evans blue dye extravasation, immunofluorescence staining, and western blotting were evaluated at 24 h after SAH induction.

Experiment 3

To elucidate the effect of DNase I treatment on EBI, 72 mice were randomly divided into three groups ($n = 24$/group): sham, SAH + vehicle (saline), and SAH + DNase I. DNase I (Roche 04,536,282,001) was dissolved in saline. DNase I (50 μg in 250 μl of saline intraperitoneally and a second dose of 10 μg intravenously) was injected 1 h after SAH induction [10]. SAH severity, neurological scores (beam balance and modified Garcia tests), brain water content, Evans blue dye

extravasation, immunofluorescence staining, and western blotting were evaluated at 24 h after SAH induction.

Experiment 4

To study the effect of DNase I treatment on CSF flow and cortical perfusion after SAH induction, 36 mice were randomly divided into the following three groups ($n = 12$/group): sham, SAH + vehicle, and SAH + DNase I. CSF EB spread assessment (cisterna magna injection) was used to evaluate CSF flow at 24 h post-SAH. A laser speckle blood monitor was used to evaluate cortical perfusion at 6 h after SAH.

Mouse SAH Model

Endovascular perforation was used to establish the SAH model as previously described [27, 28]. Briefly, the animals were anesthetized with halothane (70% N_2O and 30% O_2; 4% for induction, 2% for maintenance, RWD 21,081,501). A midline incision was made in the neck to expose the left common carotid artery, external carotid artery, and internal carotid artery. A 5–0 monofilament nylon suture was inserted into the left internal carotid artery through the external carotid artery stump to perforate the artery at the bifurcation of the anterior and middle cerebral arteries. Body temperature was kept a constant 37 °C during the operation. The mice in the sham group underwent the same procedures without the artery perforation.

SAH Grade

The SAH severity grading score was blindly evaluated by two independent investigators as previously described [29]. The basal cistern was divided into six segments, and each segment could be scored from 0 to 3 according to the amount of subarachnoid blood clotting in the segment. The total score was calculated by adding the scores from six segments (0–18 points). Mice that received a score < 8 were excluded from the study.

Neurobehavioral Test

The neurobehavioral test was blindly evaluated using the modified Garcia test and beam balance test at 24 h after SAH as previously described [30, 31]. The modified Garcia scale included six measurements as follows: spontaneous activity, forepaw outstretching, symmetry of limb climbing, responses to body proprioception, and vibrissa touch. The mice could receive a total score ranging from 3 to 18. For the beam balance score test, the mice were placed on the center of a wooden beam to assess the walking distance within 1 min and were subsequently assigned 0–4 points in total. Two blinded observers were employed for grading mean of the neurological score.

Brain Water Content

Brain edema was determined using the wet/dry method [29]. Mice were decapitated under deep anesthesia at 24 h after SAH induction. The brain samples were quickly removed from the skull, and were divided into the left and right cerebral hemispheres, the cerebellum, and the brain stem. These four parts of the brain were weighed (wet weight), respectively, and the brain samples were then dried at 55 °C for 72 h in an oven and weighed again (dry weight). The water content percentage formula was ([wet weight − dry weight]/wet weight) × 100%.

Evans Blue Extravasation

Evans blue extravasation was performed to evaluate BBB permeability as previously described [29, 32]. Mice were anesthetized by pentobarbital sodium (40 mg/kg) i.p. injection 24 h post-SAH. Evans blue dye (2%, 5 ml/kg Sigma-Aldrich, E2129) was administered into the caudal vein and circulated for 1 h. Under deep anesthesia, mice were sacrificed by intracardially perfusing with phosphate-buffered solution (PBS). The brains were removed and quickly divided into the left and right cerebral hemispheres, weighed, homogenized in PBS, and centrifuged at 15,000 g for 30 min. Subsequently, the resultant supernatant was added with an equal volume of trichloroacetic acid, and incubated overnight at 4 °C and centrifuged at 15,000 g for 30 min. Next, the resultant supernatant was collected and spectrophotometrically quantified at 610 nm for Evans blue dye.

Western Blotting

Western blotting was performed using the left cerebral cortex at 24 h after SAH as described previously [33, 34]. Equivalent (30 μg) protein amounts were loaded in SDS-PAGE gels. After gel electrophoresis, protein was transferred onto a nitrocellulose membrane, which was then blocked by blocking buffer for 2 h at room temperature. The following primary antibodies were diluted to incubate with the membrane under gentle agitation at 4 °C overnight: anti-CitH3 antibody (1:2000; Abcam; ab5103) and ZO-1 antibody (1:1000; Thermo Fisher; 40–2200). The membranes then were incubated with horseradish peroxidase–conjugated secondary antibodies for 2 h at room temperature. GAPDH (1:10,000; ZEN BIO; 200,306-7E4) was blotted on the same membrane as a loading control.

Immunofluorescence Staining

Immunofluorescence staining was performed on fixed frozen brain sections as previously described [35]. Briefly, the mice were deeply anesthetized and perfused with PBS and 4% PFA at 24 h after SAH. Brain samples were isolated and post-fixed in 4% PFA for 24 h, and then soaked in 30% sucrose for 3 days. Coronal brain Sects. (10 μm) were obtained using a cryostat (Leica, CM1860UV, Germany) and treated with 0.3% Triton for 30 min. The brain sections were subsequently blocked with 5% normal goat serum for 2 h and incubated with the primary antibodies overnight in a 4 °C freezer. The primary antibodies are listed as follows: anti-fibrinogen antibody (1:400; Abcam; ab119948), anti-CD31 antibody (1:200; Abcam; ab28364), anti-CitH3 antibody (1:200; Abcam; ab5103), and anti-Ly6G antibody (1:200; Abcam; ab25377). Then, the slices were incubated with corresponding secondary antibodies for 2 h at room temperature, followed by staining with DAPI for 5 min. Neuronal injury was detected using Fluoro-Jade C (FJC) staining according to the manufacturer's protocol (Millipore, AG325). The brain sections were successively incubated with 80% alcohol containing 1% NaOH for 5 min, 70% alcohol for 2 min, 0.06% potassium permanganate for 10 min, and 0.0004% FJC working solution for 20 min. Finally, sections were washed and dried at 42 °C for 30 min in an oven and cleared in xylene and coverslipped.

Images were obtained at the basal cortex by confocal laser scanning microscopy (Zeiss 880, Germany). We selected at least 3 slices from each mouse and analyzed three fields of per slice from similar areas of the ipsilateral cortex at a magnification of × 200. For quantification of fibrinogen-positive microthrombi, each recognizable thread-like microthrombus was counted as one regardless of its length. This resulted in a relatively lower number of total counts [6]. All the procedures were performed by two investigators who were blinded to the experimental conditions.

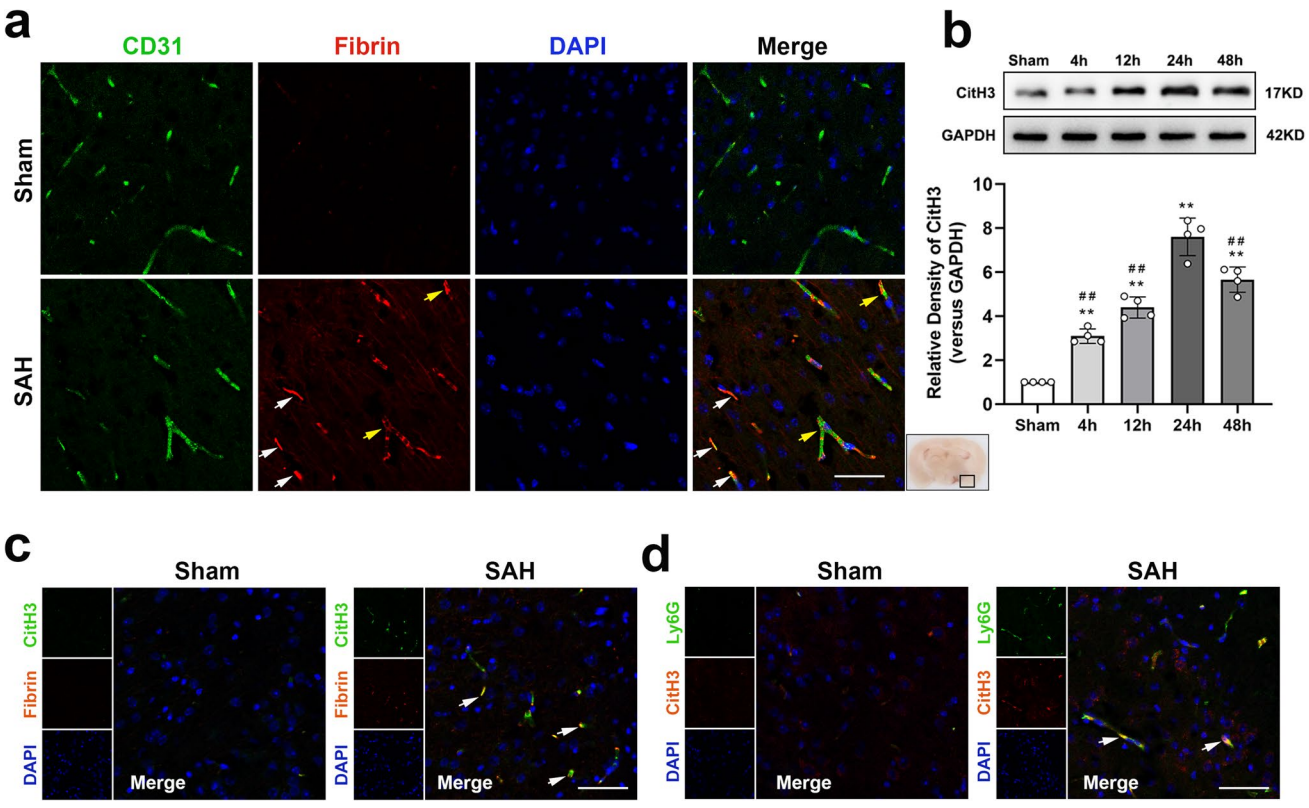

Fig. 1 Expression and distribution of NETs in the ipsilateral hemisphere after SAH. **a** Representative photographs of immunofluorescence staining for CD31 (green) and fibrinogen (red) in sham and SAH (24 h) groups. White arrows, microthrombi formed in the microvessels. Yellow arrows, microthrombi formed in the paravascular space. $n = 3$ per group. Scale bar = 50 μm. **b** Representative western blotting images and quantitative analyses of CitH3 expression in ipsilateral basal cortex after SAH. $n = 4$ per group. **c** Representative photographs of immunofluorescence staining for CitH3 (green) and fibrinogen (red) in sham and SAH (24 h) groups. $n = 3$ per group. Scale bar = 50 μm. **d** Representative photographs of immunofluorescence staining for CitH3 (red) and Ly6G (green) in sham and SAH (24 h) groups. $n = 3$ per group. Scale bar = 50 μm. Data is expressed as the mean ± *SD*. $^{**}P < 0.01$ versus sham group; $^{\#\#}P < 0.01$ versus SAH 24 h

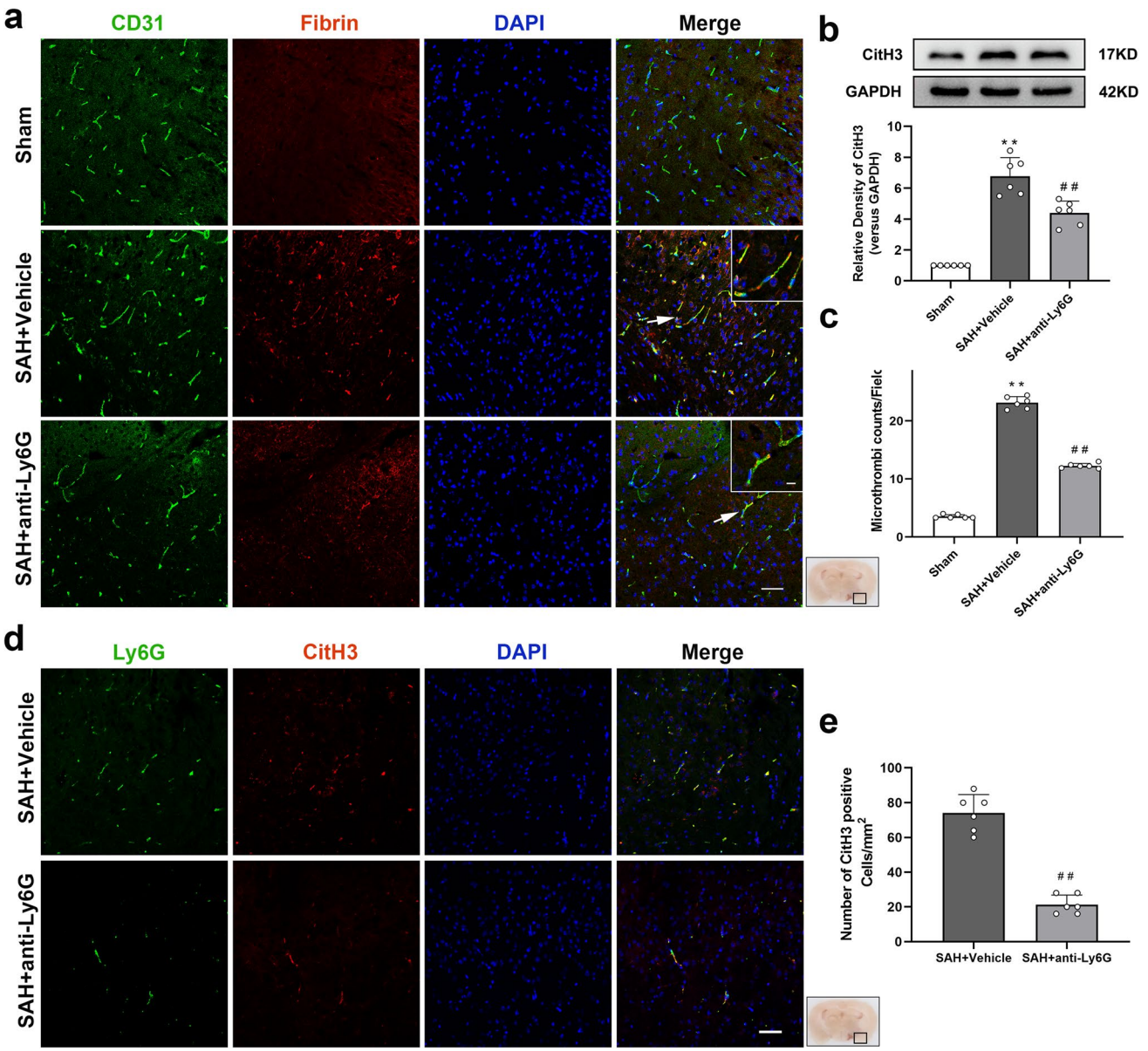

Fig. 2 Administration of anti-Ly6G antibody significantly decreased the formation of fibrinogen-positive microthrombi and NETs at 24 h after SAH. **a** Representative immunofluorescence micrographs of fibrinogen-positive microthrombi (red) with CD31 (green) in the ipsilateral basal cortex in different groups. **b** Representative western blotting images and quantitative analysis of CitH3 in the ipsilateral basal cortex in different groups. **c** Quantitative analysis of fibrinogen-positive microthrombi in different groups. **d** Representative immunofluorescence micrographs of CitH3-positive cell (red) with Ly6G (green) in the ipsilateral basal cortex in different groups. **e** Quantitative analysis of CitH3-positive cells in different groups. $n=6$ per group. Scale bar: 50 μm (overview), 10 μm (zoom-in view). Data is represented as the mean ± *SD*. $^{**}P<0.01$ versus sham group; $^{\#\#}P<0.01$ versus SAH + vehicle group

CSF Flow Assessment

Cisterna magna injection of EB dye was performed to observe the movement of CSF at 24 h after SAH as previously described [24, 36]. After anesthetization, mice were placed in the stereotaxic frame, and the atlantooccipital membrane was exposed by a midline incision. A needle (Hamilton/7803–05) was inserted 1–1.5 mm deep into the cisterna magna followed by an injection of 5 μl of 2% EB dye (Sigma-Aldrich, E2129) at rate of 1 μl/min. EB dye (2%) is prepared by dissolving EB dye in artificial cerebrospinal fluid (ACSF Tocris Bioscience 3525). After injection, the needle was kept in place for another 10 min to allow EB dye to diffuse and then withdrawn.

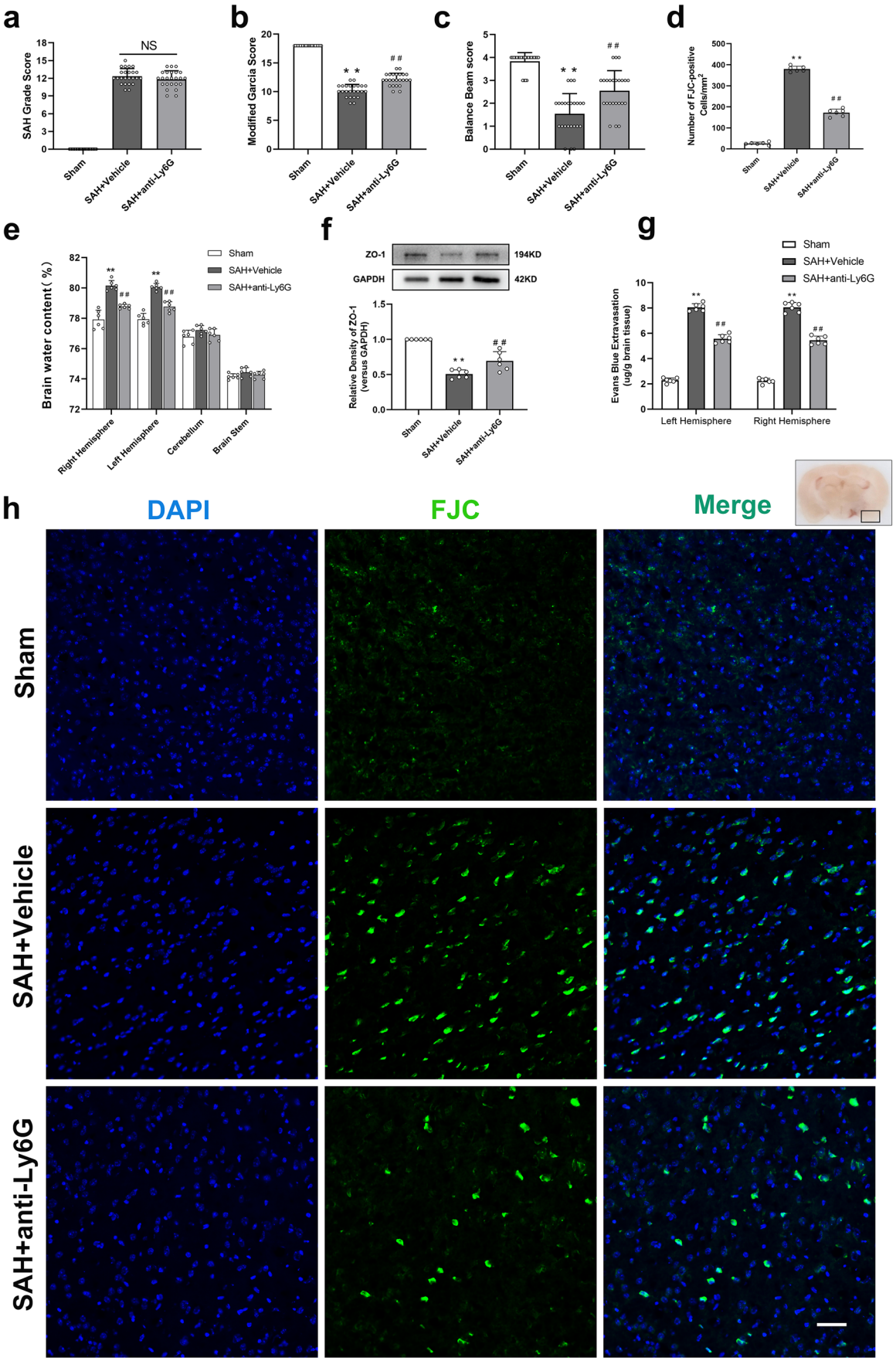
a
SAH Grade Score
NS
Sham
SAH+Vehicle
SAH+anti-Ly6G
b
Modified Garcia Score
c
Balance Beam score
d
Number of FJC-positive Cells/mm2
e
Brain water content (%)
Right Hemisphere
Left Hemisphere
Cerebellum
Brain Stem
f
ZO-1
GAPDH
194KD
42KD
Relative Density of ZO-1 (versus GAPDH)
g
Evans Blue Extravasation (ug/g brain tissue)
Left Hemisphere
Right Hemisphere
h
DAPI
FJC
Merge
Sham
SAH+Vehicle
SAH+anti-Ly6G

◂**Fig. 3** Administration of anti-Ly6G significantly attenuated neurological deficits, brain edema, BBB disruption, and neural cell injury at 24 h after SAH. **a** SAH grade score at 24 h after SAH. $n=24$ per group. **b**, **c** Modified Garcia score and balance beam score at 24 h after SAH. $n=24$ per group. **d** Quantitative analysis of FJC-positive cells in different groups. $n=6$ per group. **e** Brain water content assessment at 24 h after SAH. $n=6$ per group. **f** Representative western blotting images and quantitative analysis of ZO-1 in the ipsilateral basal cortex in different groups. $n=6$ per group. **g** Evans blue extravasation evaluation at 24 h after SAH. $n=6$ per group. **h** Representative immunofluorescence images of FJC-positive cells (green) in different groups. $n=6$ per group. Scale bar = 50 μm. Data is represented as the mean ± *SD*. $^{**}P<0.01$ versus sham group; $^{\#\#}P<0.01$ versus SAH + vehicle group. NS no statistical significance

EB dye was allowed to circulate for total of 1 h from the start of cisterna magna injection. The mice were then deeply anesthetized and perfused with PBS; brain and deep cervical lymph nodes (dcLNs) were collected. Two methods were used to quantify the EB dye distribution in the brain parenchyma and perivascular space. First, the ventral surface of the mouse brain was divided into six segments (R1–R6); each segment was given a score of 1 for dye present or 0 for no dye present, and then the score was summed. Second, the concentration of EB dye in the dcLNs and in the forebrain parenchyma (R1–R3) was quantified. The dcLNs and forebrain parenchyma were homogenized in PBS, and centrifuged at 15,000 g for 30 min. Subsequently, the resultant supernatant was added with an equal volume of trichloroacetic acid, incubated overnight at 4 °C, and centrifuged at 15,000 g for 30 min. Next, the resultant supernatant was collected and spectrophotometrically quantified at 610 nm for Evans blue dye.

Cerebral Cortical Perfusion Analysis

Cerebral cortical perfusion of the whole convexity was measured using a laser speckle blood monitor (PeriCam PSI System, Sweden) at 6 h after SAH as previously described [37, 38]. The mice were mounted on a stereotaxic frame, and a midline incision was made to expose the calvaria. Sixty perfusion images were recorded at 1 picture per second. After these measurements, the wound was then closed with sutures and anesthesia was terminated. The perfusion data were evaluated using the PIMSoft software. A mean image was calculated from the 60 perfusion images. The mean flux values were determined by evaluating a region of interest (ROI) of 7 mm^2 placed over the perfusion territory of the left middle cerebral artery [39]. Perfusion was evaluated by an investigator blinded to the treatment.

Statistical Analysis

All statistical analyses were performed using the GraphPad Prism 8 software. Quantitative data are expressed as the mean ± *SEM*. One-way ANOVA and Tukey's multiple comparisons were employed for comparisons among the different groups. The Kruskal–Wallis test was employed for the analysis of the behavior scores; $P<0.05$ was considered statistically significant.

Results

Animal Use and Mortality

A total of 255 male C57BL/6 mice were used. Ten mice were excluded due to mild SAH. None of the animals died in the sham group; 38 mice died in the modeling groups. There was no significant difference in mortality among the modeling groups. Mortality details for each group are presented in Supplementary Table 1.

The Temporal Pattern of Endogenous NET Expression and Its Localization with Microthrombi After SAH

Western blot analyses demonstrated that the level of NET marker CitH3 in the brain was significantly increased after SAH. The level of CitH3 peaked at 24 h, after which the expression of CitH3 gradually decreased ($P<0.01$) (Fig. 1b). The immunofluorescence staining was conducted at 24 h after SAH. As shown (Fig. 1a), most of the microthrombi were formed in the microvessels, and some were located in the paravascular space. Furthermore, immunofluorescence staining showed that CitH3 was co-localized with Ly6G (neutrophil marker) as well as fibrinogen-positive microthrombi (Fig. 1c, d), which suggested a correlation between NET formation and microthrombosis following SAH induction.

Anti-Ly6G Antibody Treatment Reduced NET Formation and Microthrombosis After SAH

After treatment of anti-Ly6G antibody, western blot analyses indicated that the level of CitH3 was significantly reduced in the cerebral cortex 24 h after SAH ($P<0.01$, Fig. 2b). We used immunofluorescence staining to detect NETs and microthrombosis in mouse brain tissue with vehicle or anti-Ly6G antibody administration after SAH. The results showed that a lot of fibrinogen-positive microthrombi and CitH3-positive cells appeared in the SAH + vehicle group after SAH. After intervention with anti-Ly6G antibody, microthrombi and CitH3-positive cells were significantly reduced in the SAH + anti-Ly6G group compared with those in the SAH + vehicle group ($P<0.01$, Fig. 2a, c, d, e). These results suggested that anti-Ly6G antibody

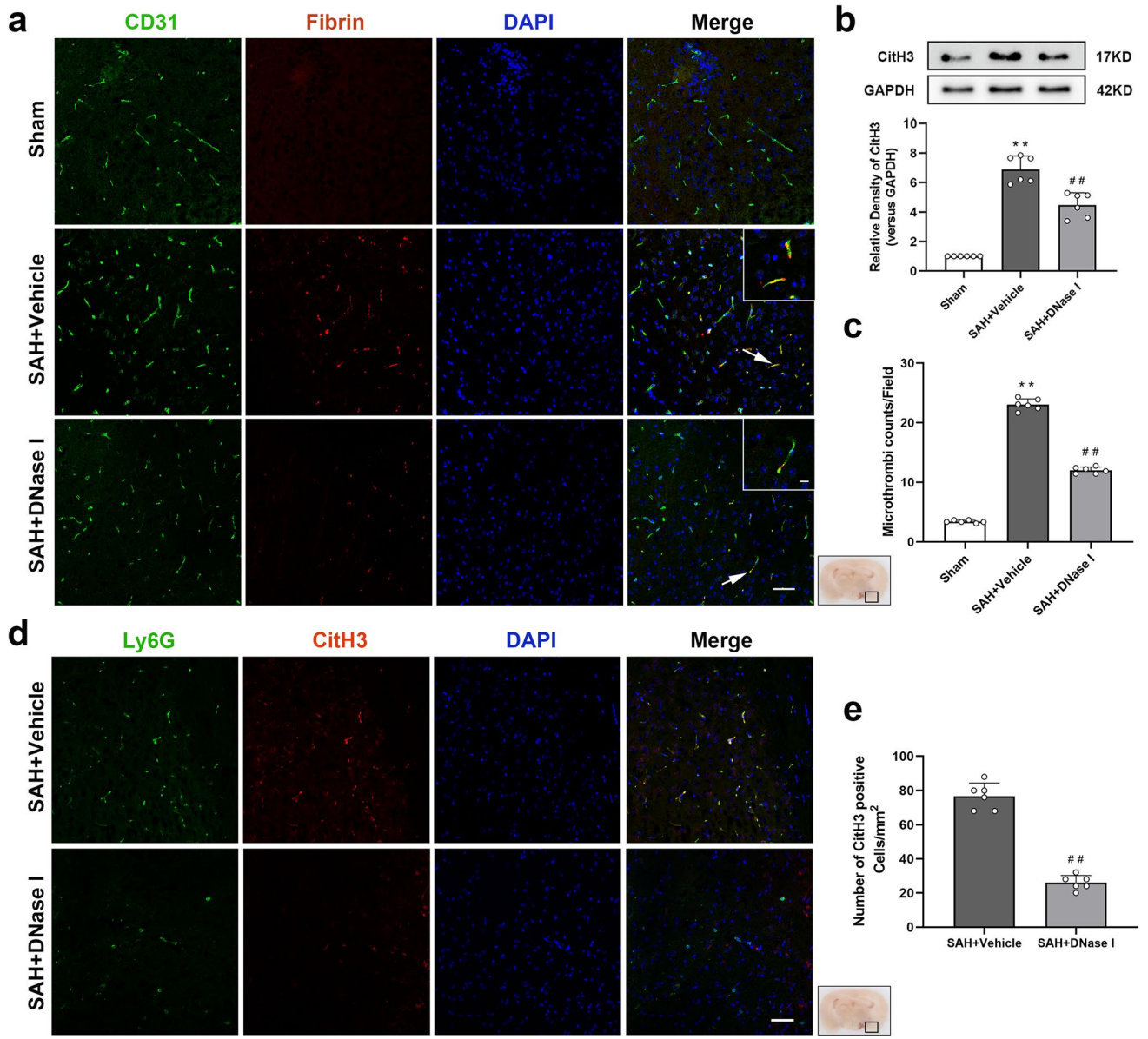

Fig. 4 Administration of DNase I significantly decreased the formation of fibrinogen-positive microthrombi and NETs at 24 h after SAH. **a** Representative immunofluorescence micrographs of fibrinogen-positive microthrombi (red) with CD31 (green) in the ipsilateral basal cortex in different groups. **b** Representative western blotting images and quantitative analysis of CitH3 in the ipsilateral basal cortex in different groups. **c** Quantitative analysis of fibrinogen-positive microthrombi in different groups. **d** Representative immunofluorescence micrographs of CitH3-positive cells (red) with Ly6G (green) in the ipsilateral basal cortex in different groups. **e** Quantitative analysis of CitH3-positive cells in different groups. $n=6$ per group. Scale bar: 50 μm (overview), 10 μm (zoom-in view). Data is represented as the mean ± *SD*. $^{**}P<0.01$ versus sham group; $^{\#\#}P<0.01$ versus SAH + vehicle group

administration reduced NET formation and microthrombosis after SAH.

Anti-Ly6G Antibody Treatment Attenuated Neurological Deficits, Brain Edema, BBB Disruption, and Neuronal Injury at 24 h After SAH

The SAH grading score results showed that there were no significant differences among the SAH + vehicle group and the SAH + anti-Ly6G group at 24 h after SAH ($P>0.05$, Fig. 3a). The modified Garcia score system and beam balance test were used to assess neurological impairment after SAH. The results showed that the modified Garcia score and beam balance score were significantly lower in the SAH + vehicle group compared to those in the sham group, while administration of anti-Ly6G antibody significantly improved neurological scores in the SAH + anti-Ly6G group ($P<0.01$, Fig. 3b, c).

The brain water content in the SAH + vehicle group was significantly increased in the bilateral hemispheres at 24 h after SAH compared with the sham group. The anti-Ly6G antibody treatments significantly decreased the brain water content in both hemispheres (both $P < 0.01$, Fig. 3e). Western blot analyses indicated that the level of ZO-1 was significantly reduced in the SAH + vehicle group; however, the administration of anti-Ly6G antibody changed this trend ($P < 0.05$, Fig. 3f). Compared with hemispheres in the sham group, the Evans blue dye extravasation was substantially higher in both hemispheres in the SAH + vehicle group, and anti-Ly6G antibody administration significantly alleviated the leakage (both $P < 0.01$, Fig. 3g).

FJC staining was performed to evaluate the neuronal injury. Compared with the sham group, hemispheres in the SAH + vehicle group exhibited a substantially increase in the number of FJC-positive cells. Anti-Ly6G antibody treatment markedly reduced the number of FJC-positive cells ($P < 0.01$, Fig. 3d, h).

DNase I Treatment Inhibits the Formation of NETs and Prevents Microthrombosis After SAH

Western blot analysis indicated that the level of NETs (CitH3 as a marker) was significantly decreased in the SAH + DNase I group compared with the SAH + vehicle group ($P < 0.01$, Fig. 4b). The results of immunofluorescence staining showed that a lot of fibrinogen-positive microthrombi and CitH3-positive cells appeared in the SAH + vehicle group. After DNase I treatment, microthrombi and the CitH3-positive cells were significantly reduced in the SAH + DNase I group ($P < 0.01$, Fig. 4a, c, d, e).

DNase I Treatment Attenuated Neurological Deficits, Brain Edema, BBB Disruption, and Neuronal Injury at 24 h After SAH

No significant difference was found in SAH grade among the SAH + vehicle group and the SAH + DNase I group at 24 h after SAH ($P > 0.05$, Fig. 5a). The modified Garcia score system and beam balance test were used to assess neurological impairment after SAH. The results showed that the modified Garcia score and beam balance score were significantly lower in the SAH + vehicle group compared to those in the sham group; however, administration of DNase I notably improved neurological scores in the SAH + DNase I group ($P < 0.01$, Fig. 5b, c). Western blotting analysis showed that the expressions of ZO-1 decreased in the SAH + vehicle group compared to those in the sham group. DNase I treatment prevented these reductions ($P < 0.01$, Fig. 5f). Moreover, DNase I treatment substantially alleviated brain edema and Evans blue dye extravasation at 24 h after SAH ($P < 0.01$, Fig. 5e, g).

FJC staining was performed to evaluate the neuronal injury. Hemispheres in the SAH + vehicle group showed a significant increase in the number of FJC-positive cells compared to those in the sham group, and DNase I treatment markedly reduced the number of FJC-positive cells ($P < 0.01$, Fig. 5d, h).

DNase I Treatment Attenuated CSF Flow Dysfunction at 24 h After SAH

At 1 h after cisterna magna injection, EB dye was grossly visible on the ventral surface of the mouse brain in the sham group. The spread of EB dye was impaired in the SAH + vehicle group, but was improved by DNase I treatment (Fig. 6a). The number of EB-positive region and EB dye concentration in the forebrain decreased significantly in the SAH + vehicle group when compared with the sham group, and DNase I treatment significantly improved such impairment of CSF movement when compared with the SAH + vehicle group ($P < 0.01$, Fig. 6b, e).

Furthermore, the dcLN EB concentration suggested that SAH significantly blocked the clearance of EB dye from the subarachnoid space to dcLNs 1 h after EB dye cisterna injection. Meanwhile, the DNase I treatment significantly accelerated the clearance of EB dye from the CSF to dcLNs compared with the SAH + vehicle group ($P < 0.01$, Fig. 6d).

DNase I Treatment Improved Recovery of Early Cortical Hypoperfusion After SAH

Laser speckle blood monitoring was used to determine cortical perfusion 6 h after SAH. Cortical blood flow in the left middle cerebral artery region was significantly decreased in SAH + vehicle group after 6 h of SAH induction, while in the SAH + DNase I group, it recovered significantly at the same time point ($P < 0.01$, Fig. 6f, g).

Discussion

Recently, microthrombosis has been reported to be a potential target for treating early brain injury after SAH [5, 18]. However, little is known about the mechanism

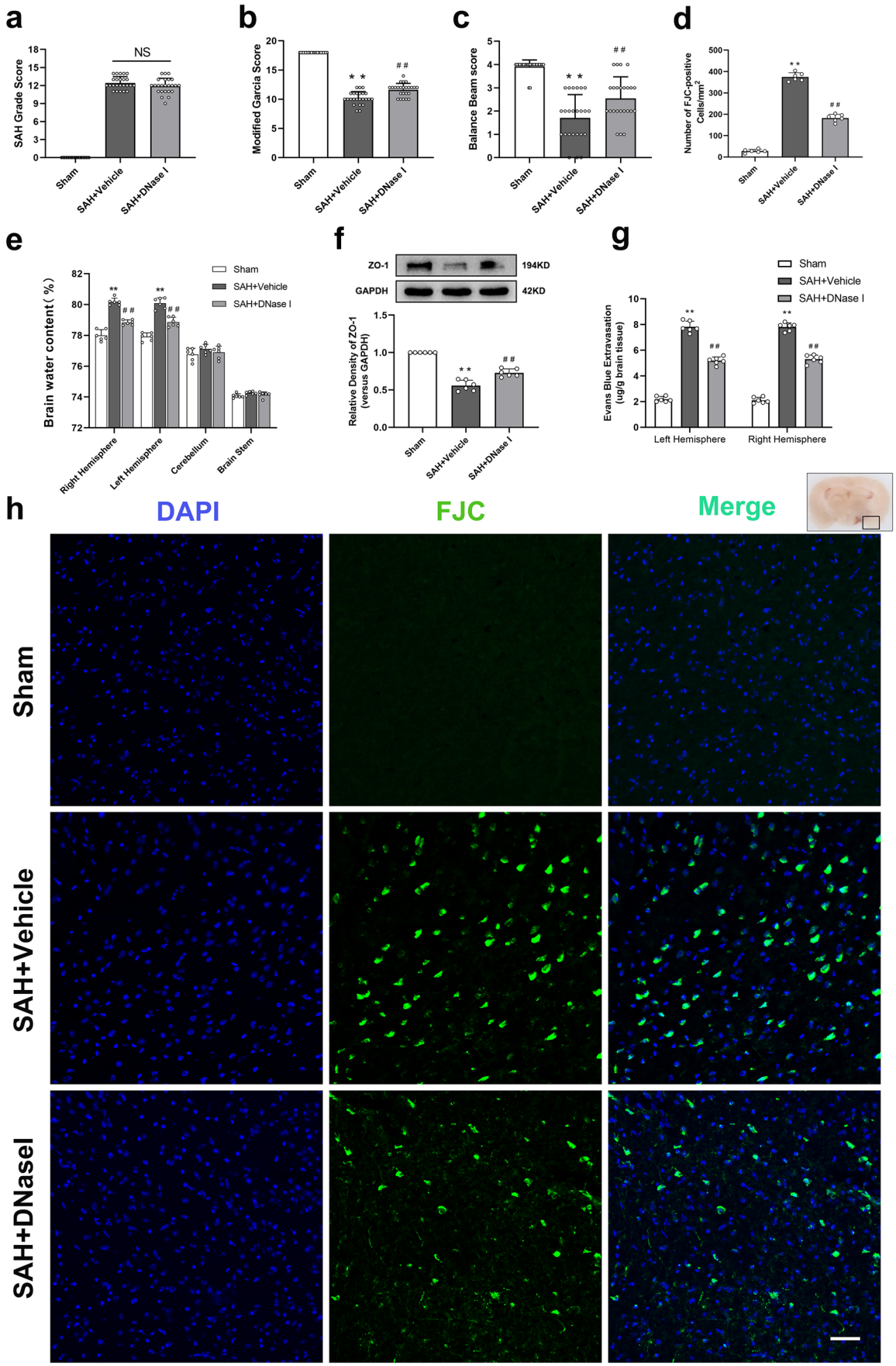
a
SAH Grade Score
NS
Sham
SAH+Vehicle
SAH+DNase I
b
Modified Garcia Score
c
Balance Beam score
d
Number of FJC-positive Cells/mm2
e
Brain water content (%)
Right Hemisphere
Left Hemisphere
Cerebellum
Brain Stem
f
ZO-1
194KD
GAPDH
42KD
Relative Density of ZO-1 (versus GAPDH)
g
Evans Blue Extravasation (ug/g brain tissue)
Left Hemisphere
Right Hemisphere
h
DAPI
FJC
Merge
Sham
SAH+Vehicle
SAH+DNasel

◂**Fig. 5** Administration of DNase I significantly attenuated neurological deficits, brain edema, BBB disruption, and neural cell injury at 24 h after SAH. **a** SAH grade score at 24 h after SAH. $n=24$ per group. **b**, **c** Modified Garcia score and balance beam score at 24 h after SAH. $n=24$ per group. **d** Quantitative analysis of FJC-positive cells in different groups. $n=6$ per group. **e** Brain water content assessment at 24 h after SAH. $n=6$ per group. **f** Representative western blotting images and quantitative analysis of ZO-1 in the ipsilateral basal cortex in different groups. $n=6$ per group. **g** Evans blue extravasation evaluation at 24 h after SAH. $n=6$ per group. **h** Representative immunofluorescence images of FJC-positive cells (green) in different groups. $n=6$ per group. Scale bar = 50 μm. Data is represented as the mean ± *SD*. $^{**}P<0.01$ versus sham group; $^{\#\#}P<0.01$ versus SAH + vehicle group. NS no statistical significance

of microthrombosis after SAH. In this study, we were the first to demonstrate a robust correlation between NETs and the microthrombosis after SAH. We observed the following findings: (1) The expression of CitH3, the biomarker of NETs, was significantly increased in the mouse brain and peaked at 24 h after SAH modeling; it mainly located in neutrophils and co-located with fibrinogen-positive microthrombi. (2) Anti-Ly6G antibody as well as DNase I treatment reduced NET formation and microthrombosis and significantly alleviated early brain injury after SAH. (3) DNase I treatment attenuated CSF flow dysfunction at 24 h after SAH. It also improved recovery of early cortical hypoperfusion after SAH.

NETs were first described in 2004; previous research has demonstrated that NETs were involved in thrombosis [12, 13, 40]. In 2017, Laridan et al. demonstrated the presence of NETs in ischemic stroke thrombi [41]. In current study, for the first time, NETs was found co-located with fibrinogen-positive microthrombi after SAH. Depletion of neutrophils by anti-Ly6G antibody reduces NET formation, reduces microthrombosis, and attenuates early brain injury after SAH. This result indirectly supports the hypothesis that NETs were involved in the formation of microthrombi after SAH. Although anti-Ly6G antibody administration reduces early brain injury after SAH, the translational value of this global neutrophil depletion is limited by the development of associated side effects [42, 43].

Given the lack of effective treatment to reduce microthrombosis, NETs may provide a previously unrecognized effective target to limit the deleterious consequences while preserving the beneficial aspects of neutrophils after SAH. NETs are fibrous networks of extracellular DNA released by neutrophils under the form of decondensed chromatin associated with neutrophil granule proteins and histones, which contribute to platelet aggregation and thrombus formation [40, 44]. Recent studies showed that administration of DNase I, which degrades extracellular DNA and thereby NETs, improves outcome after myocardial infarction and ischemic stroke in mice [41, 45, 46]. Our research also demonstrated DNase I as a potential therapeutic target for preventing formation of microthrombi after SAH. Infusion of DNase I significantly inhibited the formation of NETs, microthrombosis, brain edema, neuronal injury, and BBB disruption.

Previous studies have demonstrated a high relevance between early cerebral hypoperfusion and poor outcome after SAH, and microvascular thrombosis may be an important cause of cerebral hypoperfusion after SAH [39]. This is in line with our study. When microthrombosis was inhibited by DNase I treatment after SAH, the cerebral cortical perfusion was significantly improved.

CSF blocks are among the serious neurological complications after SAH, which can directly lead to cerebral edema and hydrocephalus [47]. However, the mechanism responsible for this blockade is still not fully understood. Previous research has suggested it may be associated with excessive fibrinogen deposition in the paravascular space remote from the hemorrhage, where no visible blood was present [48]. In our study, fibrinogen-positive microthrombi were also found in the paravascular space. Dissolving NETs by DNase I treatment improved the recovery of CSF flow after SAH. This result suggests that the formation of NETs after SAH is associated with impairment of CSF flow.

Nevertheless, this study has limitations. First, the role of NETs in microthrombosis was only investigated within 24 h after SAH. It may be more valuable to select more research time points. Previous studies suggested that delayed cerebral ischemia (DCI) was one of the main causes of poor prognosis after SAH, and microthrombosis was proposed as one of the key mechanisms in DCI [49]. The long-term effects of NETS should also be examined in the future to further understand its role in microthrombosis after SAH. In addition, in this study, we observed the effect of NETs on CSF flow, but the specific mechanism was not been elucidated. Therefore, further studies are needed to elucidate the role and mechanisms of NETs in SAH.

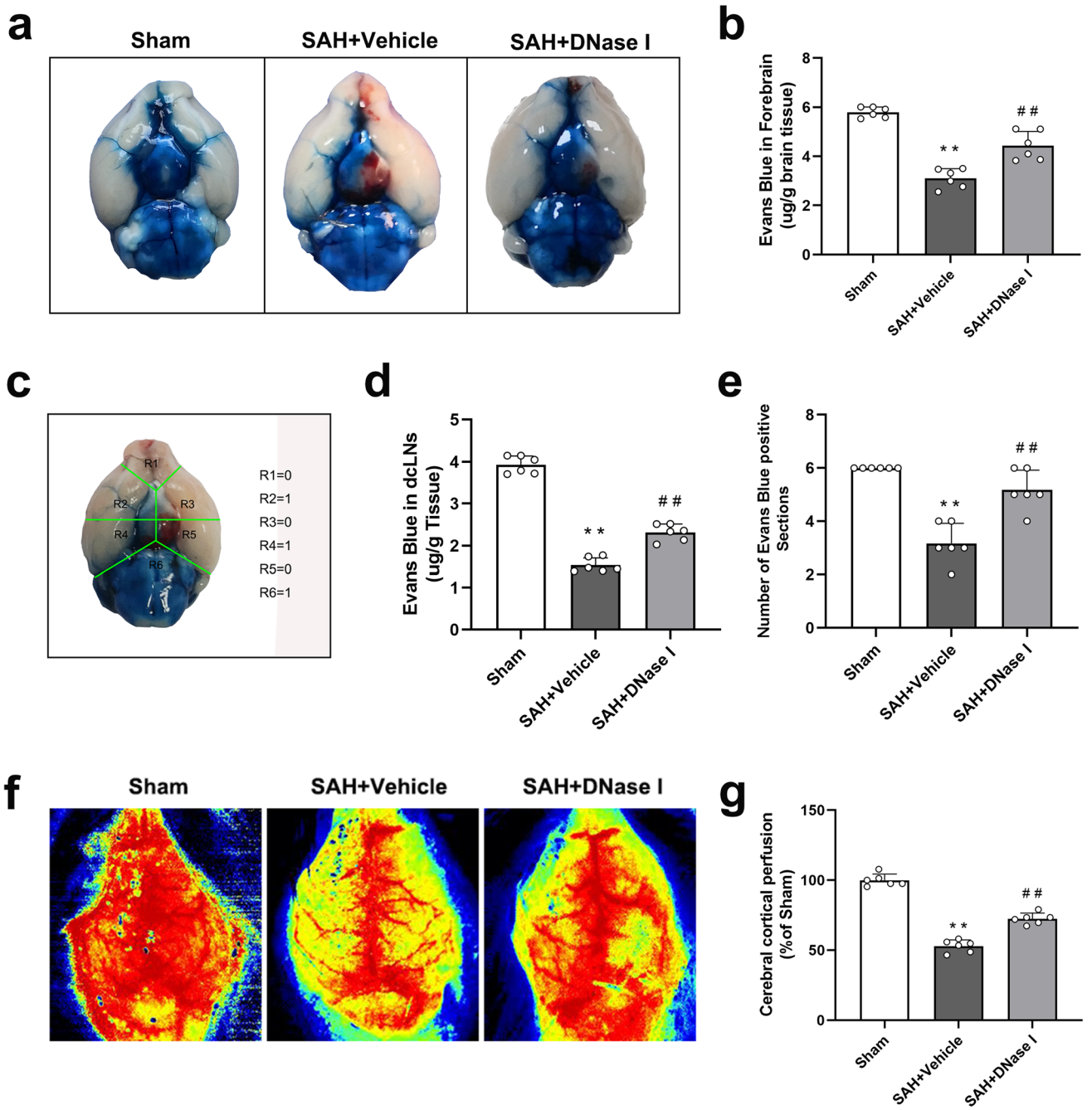

Fig. 6 Administration of DNase I attenuated CSF flow disorder and improved cerebral cortical perfusion after SAH. **a** Representative image of Evans blue distribution in the ventral surface subarachnoid space 1 h after Evans blue (2%) injection into cisterna magna. **b** Concentration of Evans blue (μg/g brain tissue) in the forebrain. **c** The ventral brain was divided into six segments. **d** Concentration of Evans blue (μg/g tissue) in the dcLNs. **e** Quantification of Evans blue–positive section on the ventral brain. **f** Representative cerebral cortical perfusion images of the mouse in different groups 6 h post-SAH. **g** Quantification of cerebral cortical perfusion at 6 h post-SAH. $n=6$ per group. Data is represented as the mean ± *SD*. $^{**}P<0.01$ versus sham group; $^{\#\#}P<0.01$ versus SAH + vehicle group

Conclusion

Our study demonstrated that the formation of NETs contributed to the microthrombosis after SAH. Inhibiting NETs reduced microthrombosis, thereby attenuated EBI, reduced CSF flow, and improved the recovery of cortical perfusion. Therefore, NETs may be a novel therapeutic target for microthrombosis after SAH and provide a multipotent therapeutic strategy for the treatment of EBI after SAH.

Supplementary Information The online version contains supplementary material available at https://doi.org/10.1007/s12975-022-01074-9.

Author Contribution XH, ZC, YC, and HF contributed to the conception and experimental design. XH, BX, and PG performed the SAH modeling and western blots. XH, ZZ, LL, ZF, WL, and QZ performed the rest of the experiments, analyzed data, and interpreted the experimental results. XH and ZC drafted the manuscript. All authors read and approved the final version of the manuscript.

Funding This study was supported by the National Natural Science Foundation of China (Grant No. 81771241 to Z.C.).

Data Availability All raw data used in this manuscript are available on reasonable request.

Declarations

Ethics Approval and Consent to Participate All experimental procedures involving animals were approved by the Ethics Committee of the Army Medical University (Third Military Medical University), and were performed in accordance with the guidelines in the National Institutes of Health (NIH) Guide for the Care and Use of Laboratory Animals, and followed the ARRIVE guidelines. This article does not contain any studies with human participants performed by any of the authors.

Consent for Publication The manuscript is approved by all authors for publication.

Conflict of Interest The authors declare no competing interests.

References

1. Connolly ES Jr, et al. Guidelines for the management of aneurysmal subarachnoid hemorrhage: a guideline for healthcare professionals from the American Heart Association/American Stroke Association. Stroke. 2012;43(6):1711–37.
2. Zeng H, et al. Neutrophil extracellular traps may be a potential target for treating early brain injury in subarachnoid hemorrhage. Transl Stroke Res. 2022;13(1):112–31.
3. Sabri M, Lass E, Macdonald RL. Early brain injury: a common mechanism in subarachnoid hemorrhage and global cerebral ischemia. Stroke Res Treat. 2013;2013:394036.
4. Fujii M, et al. Early brain injury, an evolving frontier in subarachnoid hemorrhage research. Transl Stroke Res. 2013;4(4):432–46.
5. Clarke JV, et al. Microvascular platelet aggregation and thrombosis after subarachnoid hemorrhage: a review and synthesis. J Cereb Blood Flow Metab. 2020;40(8):1565–75.
6. Sabri M, et al. Mechanisms of microthrombi formation after experimental subarachnoid hemorrhage. Neuroscience. 2012;224:26–37.
7. Friedrich B, et al. Experimental subarachnoid hemorrhage causes early and long-lasting microarterial constriction and microthrombosis: an in-vivo microscopy study. J Cereb Blood Flow Metab. 2012;32(3):447–55.
8. Ye F, et al. Acute micro-thrombosis after subarachnoid hemorrhage: A new therapeutic target? J Cereb Blood Flow Metab. 2021;41(9):2470–2472.
9. Guo Y, Zeng H, Gao C. The role of neutrophil extracellular traps in central nervous system diseases and prospects for clinical application. Oxid Med Cell Longev. 2021;2021:9931742.
10 Vaibhav K, et al. Neutrophil extracellular traps exacerbate neurological deficits after traumatic brain injury. Sci Adv. 2020;6(22):eaax8847.
11. Garcia-Culebras A, et al. Role of TLR4 (Toll-like receptor 4) in N1/N2 neutrophil programming after stroke. Stroke. 2019;50(10):2922–32.
12. Fuchs TA, et al. Extracellular DNA traps promote thrombosis. Proc Natl Acad Sci U S A. 2010;107(36):15880–5.
13. Martinod K, Wagner DD. Thrombosis: tangled up in NETs. Blood. 2014;123(18):2768–76.
14. von Bruhl ML, et al. Monocytes, neutrophils, and platelets cooperate to initiate and propagate venous thrombosis in mice in vivo. J Exp Med. 2012;209(4):819–35.
15. Varady CBS, et al. Recombinant human DNase I for the treatment of cancer-associated thrombosis: a pre-clinical study. Thromb Res. 2021;203:131–7.
16. Middleton EA, et al. Neutrophil extracellular traps contribute to immunothrombosis in COVID-19 acute respiratory distress syndrome. Blood. 2020;136(10):1169–79.
17. Neulen A, et al. Neutrophils mediate early cerebral cortical hypoperfusion in a murine model of subarachnoid haemorrhage. Sci Rep. 2019;9(1):8460.
18. Ye F, et al. Acute micro-thrombosis after subarachnoid hemorrhage: a new therapeutic target? J Cereb Blood Flow Metab. 2021;41(9):2470–2.
19. Klimo P Jr, et al. Marked reduction of cerebral vasospasm with lumbar drainage of cerebrospinal fluid after subarachnoid hemorrhage. J Neurosurg. 2004;100(2):215–24.
20. Gaberel T, et al. Impaired glymphatic perfusion after strokes revealed by contrast-enhanced MRI: a new target for fibrinolysis? Stroke. 2014;45(10):3092–6.
21. Iliff JJ, et al. A paravascular pathway facilitates CSF flow through the brain parenchyma and the clearance of interstitial solutes, including amyloid beta. Sci Transl Med. 2012;4(147):147ra111.
22. Mestre H, et al. Aquaporin-4-dependent glymphatic solute transport in the rodent brain. Elife. 2018;7:e40070.
23. Dissing-Olesen L, Hong S, Stevens B. New brain lymphatic vessels drain old concepts. EBioMedicine. 2015;2(8):776–7.
24. Siler DA, et al. Intracisternal administration of tissue plasminogen activator improves cerebrospinal fluid flow and cortical perfusion after subarachnoid hemorrhage in mice. Transl Stroke Res. 2014;5(2):227–37.
25. Wong SL, et al. Diabetes primes neutrophils to undergo NETosis, which impairs wound healing. Nat Med. 2015;21(7):815–9.
26. Provencio JJ, et al. Neutrophil depletion after subarachnoid hemorrhage improves memory via NMDA receptors. Brain Behav Immun. 2016;54:233–42.
27. Nishikawa H, et al. Modified citrus pectin prevents blood-brain barrier disruption in mouse subarachnoid hemorrhage by inhibiting galectin-3. Stroke. 2018;49(11):2743–51.
28. Buhler D, Schuller K, Plesnila N. Protocol for the induction of subarachnoid hemorrhage in mice by perforation of the circle of Willis with an endovascular filament. Transl Stroke Res. 2014;5(6):653–9.
29. Li G, et al. NEK7 coordinates rapid neuroinflammation after subarachnoid hemorrhage in mice. Front Neurol. 2020;11:551.
30. Fujimoto M, et al. Deficiency of tenascin-C and attenuation of blood-brain barrier disruption following experimental subarachnoid hemorrhage in mice. J Neurosurg. 2016;124(6):1693–702.
31. Pang J, et al. Inhibition of blood-brain barrier disruption by an apolipoprotein E-mimetic peptide ameliorates early brain injury

in experimental subarachnoid hemorrhage. Transl Stroke Res. 2017;8(3):257–72.
32. Pan P, et al. Cyclosporine A alleviated matrix metalloproteinase 9 associated blood-brain barrier disruption after subarachnoid hemorrhage in mice. Neurosci Lett. 2017;649:7–13.
33. Liu L, et al. Role of periostin in early brain injury after subarachnoid hemorrhage in mice. Stroke. 2017;48(4):1108–11.
34. Li B, et al. Progranulin reduced neuronal cell death by activation of sortilin 1 signaling pathways after subarachnoid hemorrhage in rats. Crit Care Med. 2015;43(8):e304–11.
35. Zuo S, et al. Artesunate protected blood-brain barrier via sphingosine 1 phosphate receptor 1/phosphatidylinositol 3 kinase pathway after subarachnoid hemorrhage in rats. Mol Neurobiol. 2017;54(2):1213–28.
36. Fang Y, et al. Pituitary adenylate cyclase-activating polypeptide attenuates brain edema by protecting blood-brain barrier and glymphatic system after subarachnoid hemorrhage in rats. Neurotherapeutics. 2020;17(4):1954–72.
37. Liu Q, et al. Impaired meningeal lymphatic vessels exacerbate early brain injury after experimental subarachnoid hemorrhage. Brain Res. 2021;1769:147584.
38. Chen X, et al. Tauroursodeoxycholic acid prevents ER stress-induced apoptosis and improves cerebral and vascular function in mice subjected to subarachnoid hemorrhage. Brain Res. 2020;1727:146566.
39. Neulen A, et al. Large vessel vasospasm is not associated with cerebral cortical hypoperfusion in a murine model of subarachnoid hemorrhage. Transl Stroke Res. 2018;10(3):319–326.
40. Brinkmann V, et al. Neutrophil extracellular traps kill bacteria. Science. 2004;303(5663):1532–5.
41. Laridan E, et al. Neutrophil extracellular traps in ischemic stroke thrombi. Ann Neurol. 2017;82(2):223–32.
42. Kenne E, et al. Neutrophil depletion reduces edema formation and tissue loss following traumatic brain injury in mice. J Neuroinflammation. 2012;9:17.
43. Uhl MW, et al. Effects of neutropenia on edema, histology, and cerebral blood flow after traumatic brain injury in rats. J Neurotrauma. 1994;11(3):303–15.
44. Massberg S, et al. Reciprocal coupling of coagulation and innate immunity via neutrophil serine proteases. Nat Med. 2010;16(8):887–96.
45. Ducroux C, et al. Thrombus neutrophil extracellular traps content impair tPA-induced thrombolysis in acute ischemic stroke. Stroke. 2018;49(3):754–7.
46. Savchenko AS, et al. VWF-mediated leukocyte recruitment with chromatin decondensation by PAD4 increases myocardial ischemia/reperfusion injury in mice. Blood. 2014;123(1):141–8.
47. Fang Y, et al. Inhibition of caspase-1-mediated inflammasome activation reduced blood coagulation in cerebrospinal fluid after subarachnoid haemorrhage. EBioMedicine. 2022;76:103843.
48. Golanov EV, et al. Subarachnoid hemorrhage - induced block of cerebrospinal fluid flow: role of brain coagulation factor III (tissue factor). J Cereb Blood Flow Metab. 2018;38(5):793–808.
49. Wang J, et al. Recombinant human milk fat globule-epidermal growth factor 8 attenuates microthrombosis after subarachnoid hemorrhage in rats. J Stroke Cerebrovasc Dis. 2020;29(3):104536.